Lift Enhancement on Oscillating Airfoils

D.J. Cleaver[*], Z. Wang[†], and I. Gursul[‡]
University of Bath, Bath, BA2 6AH, United Kingdom

Force and particle image velocimetry measurements were conducted on a NACA 0012 airfoil undergoing sinusoidal plunge oscillations at amplitudes of 2.5% to 20% of chord, a post-stall angle of attack of 15°, and Reynolds number of 10,000. It was shown that airfoil oscillations significantly increase lift and reduce drag. Lift improvement is primarily due to the formation of a strong leading edge vortex on the upper surface. At lower Strouhal numbers this leading edge vortex is shed and convects into the wake, interacting destructively with the trailing edge vortices. Within this regime the lift coefficient increases approximately linearly with plunge velocity. At higher Strouhal numbers the upper surface leading edge vortex remains nearer the leading-edge of the airfoil and is therefore dissipated through the rising motion of the airfoil, whilst on the lower surface a leading edge vortex forms that acts to detract from the lift force. As a result a fall in lift is observed. Local maxima were observed in the lift curves at specific Strouhal numbers for all amplitudes and also for a higher Reynolds number. It was postulated that the peak at a Strouhal number of 0.5 could be due to the vortex convection time scale, however this does not explain the other peaks. A second hypothesis is that all the maxima are due to resonance with the most unstable wake frequency, its subharmonic and harmonics.

Nomenclature

a	=	amplitude of plunging motion
C_d	=	time-averaged drag coefficient
C_l	=	time-averaged lift coefficient
c	=	chord length
f	=	frequency
Re	=	Reynolds number, $\rho U_\infty c/ \mu$
Sr_A	=	Strouhal number based on double-amplitude, $2fa/U_\infty$
Sr_c	=	Strouhal number based on chord, fc/U_∞
Sr_d	=	Strouhal number based on vertical distance between leading and trailing edge, $fc\sin\alpha/U_\infty$
t	=	time, t = 0 is top of motion
T	=	plunge period
U_∞	=	free stream velocity
α	=	angle of attack
Γ	=	circulation
μ	=	viscosity
ρ	=	density
ω	=	vorticity

I. Introduction

There is currently growing interest in the field of Micro Air Vehicles (MAVs) due to their potential for a wide variety of applications, both military and civil. The requirements for these applications can generally be subdivided into three categories: long-endurance, short-endurance with hover, and maneuverability with hover. Current designs are incapable of satisfying the requirements for any of these categories[1]. Rotary designs are

[*] Postgraduate Student, Department of Mechanical Engineering.
[†] RCUK Academic Fellow, Department of Mechanical Engineering.
[‡] Professor, Department of Mechanical Engineering. Associate Fellow AIAA.

generally too inefficient, flapping wing designs too complex, and fixed-wing designs too inefficient and inherently incapable of hover. Fixed-wing designs, or derivations thereof, have however come close to satisfying the long-endurance criteria. In fact, of the three designs identified by Pines & Bohorquez[1] as having the longest endurance all are fixed-wing. Current fixed-wing designs rely heavily on steady-state aerodynamics which become particularly inefficient at the low Reynolds numbers typical of MAVs[2]. A viable solution could therefore be to enhance the performance of fixed-wing designs through unsteady aerodynamics[3, 4].

One possible solution is to take the simplest lift enhancement mechanism from nature, the leading edge vortex, and apply it in a way suited to the current technology, i.e., instead of the large-amplitude, low-frequency plunging motion that is suited to muscular actuators, utilize small-amplitude, high-frequency motion which is more suited to electric motors or piezoelectric actuators. The simplicity of this approach allows it to be both mechanically less complex, and removes the need for complex control systems. Indeed it is feasible that this motion could be passively produced through aeroelastic interaction as has previously[5] been demonstrated for delta wings.

Both experiments[6] and computational simulations[7] of small-amplitude high-frequency plunge motion on two-dimensional airfoils have demonstrated significant performance improvements, i.e., separation reduction and thrust enhancement. These improvements were achieved through the action of leading and trailing edge vortices. At small Strouhal numbers a leading edge vortex forms and is shed over the upper surface during the downward motion, convecting over the upper surface and thereby enhancing mixing, and reducing the separated region. This was termed a mode-1 flow field. At higher Strouhal numbers the lift-enhancing leading edge vortex is dissipated through impingement with the upward moving airfoil. This was termed a mode-2 flow field. Due to the LEV dissipation one would presume that any extra performance improvements are diminished, effectively creating an upper frequency limit, however no force data was presented in the previous work to substantiate this.

This paper provides both force and PIV data that will demonstrate the potential gains and limitations of small-amplitude high-frequency plunging motion. It is built around a central case of a NACA 0012 airfoil at a fixed angle of attack $\alpha = 15°$ and Reynolds number of 10,000, plunging at an amplitude of 15%c. Other Reynolds numbers (Re = 20,000) and amplitudes (2.5%c to 20%c) are also considered. Further experimental results for pre-stall angles of attack shall be presented in a future paper.

II. Experimental Apparatus and Procedures

Force and PIV measurements were conducted on a sinusoidally plunging NACA 0012 airfoil mounted vertically in a closed-loop water tunnel. For a review of parameters studied, see Table 1; uncertainties are calculated based on the methods of Moffat[8]. Force uncertainties were calculated for all data points taking into account both bias and precision errors, however for convenience only typical examples are shown in Table 1.

Table 1 Experimental Parameters

Parameter	Range Considered	Uncertainty
Re	10,000 to 20,000	+/- 200
α	15°	+/- 0.5°
a/c	0.025 to 0.200	+/- 0.003
Sr_c	0 to 3	+/- 2.3%
C_l	0.7 to 2.5	+/- 0.03 to 0.13
C_d	0.5 to -3	+/- 0.04 to 0.09

A. Experimental Setup

The experiments were conducted in a free-surface closed-loop water tunnel (Eidetics Model 1520) at the University of Bath. The water tunnel is capable of flow speeds in the range 0 to 0.5 m/s and has a working section of dimensions 381 mm x 508 mm x 1530 mm. The turbulence intensity has previously[9] been measured by LDV to be less than 0.5%.

A NACA 0012 airfoil of 0.1 m chord x 0.3 m span was mounted vertically in a 'shaker' mechanism, see Fig. 1. The airfoil was constructed by rapid prototyping from SLS Duraform Prototype PA. It was placed between an upper and lower splitter plate, clearances were maintained at less than 2 mm. The plunging motion is defined in Fig. 2. PIV, flow visualization and force measurements showed static stall to commence at $\alpha = 10°$. This is in agreement with previous studies at comparable Reynolds numbers[10-14].

The oscillations were supplied via a Motavario 0.37 kW three-phase motor, 5:1 wormgear and IMO Jaguar Controller. The position of the root of the airfoil was measured through a rotary encoder attached to the spindle of the worm gear shaft. The rotary encoder was also used to trigger the PIV system.

B. Force Measurements

The forces applied in both the parallel and perpendicular directions were measured via a two-component aluminium binocular strain gauge force balance[15]. The measured forces included both time-dependent aerodynamic forces as well as inertia forces, however through time-averaging the inertia forces are eliminated. In this study only the time-averaged lift and time-averaged drag are considered as this is sufficient to characterize any performance gains.

One of the inherent deficiencies of this force measurement technique is that to function a strain must be produced, thereby introducing flexibility. Due to the forces being roughly proportional to the frequency squared, the forces experienced at $Sr_c = 3$ were approximately nine times the forces at $Sr_c = 1$. A force balance designed for use at $Sr_c = 1$ would therefore produce excessively large displacements at $Sr_c = 3$, and one designed for $Sr_c = 3$ would be inaccurate at $Sr_c = 1$. Three force balances were therefore used of varying rigidities. Measurements were taken multiple times across the entire frequency range, using all three force balances so as to validate each other. Generally the agreement between the three was extremely good.

The signal from the strain gauges was amplified by a Wheatstone bridge circuit and sampled at either 2 kHz for 20,000 samples (static cases), or 360/cycle for a minimum of 50 cycles (dynamic cases). Each data point was taken a minimum of two times and the forces calculated from the average voltage through linear calibration curves. To minimize uncertainty the calibration curves consisted of twenty three points, and were performed daily before and after testing.

C. PIV Measurements

A TSI 2D-PIV system was used to measure the velocity field in the vicinity of the airfoil. For measurements over the upper surface of the airfoil, the laser was positioned behind as shown in Fig. 1. The shadow created by the airfoil therefore obscured the lower surface. For measurements over the lower surface the laser was positioned near the side wall of the tunnel. In both cases, the camera was located under the tunnel as shown in Fig. 1. The PIV images were analyzed using the software Insight 3G. A recursive FFT correlator was selected to generate a vector field of 199 x 148 vectors giving a 1.22 mm spatial resolution for the upper surface, and 0.88 mm for the lower surface. The phase-averaged data is derived from 100 pairs for the upper surface and between 100 and 250 pairs (as required) for the lower surface. The upper and lower surface data were later merged through interpolation of the lower surface data onto the upper surface grid in MATLAB. For the central case phase-averaged data was taken at eight points throughout the cycle and animated, however for convenience only the top and bottom of the motion are shown herein.

To calculate the circulation from the phase-averaged data, first the vortex is located using a vortex identification algorithm[16, 17] with the search centered on the point of maximum / minimum vorticity as appropriate. The radius of the vortex is then determined by continually expanding from the centre, one spatial resolution unit at a time, until the increase in circulation is negative or small (<1%). The circulation calculation itself is done using both line integral and vorticity surface methods[18]. The agreement between the two was generally very good. All circulation results presented herein are derived from the average of the two methods, normalized according to Eq. (1):

$$\hat{\Gamma} = \frac{\Gamma}{U_\infty c} \tag{1}$$

It was not possible to perform circulation calculations for Strouhal numbers below $Sr_c = 0.375$ as the vortex was too weak or indistinct.

III. Results & Discussion

A. Lift Enhancement

Figure 3 shows the time-averaged lift coefficient and Fig. 4 the time-averaged drag coefficient for the central case: a/c = 0.15 and Re = 10,000. The dashed lines denote the Strouhal number limits for the regions of phased-averaged PIV data shown in Figs 5 to 8. Figure 3 demonstrates significant lift enhancement with increasing Strouhal number until a sudden fall in lift at higher Strouhal numbers. Before the fall in lift occurs two peaks in the time-

averaged lift are observed at $Sr_c \sim 0.5$ and 1.25. These peaks are reflected in the drag variation shown in Fig. 4. In addition Fig. 4 demonstrates the well documented[19-21] switch from drag to thrust at $Sr_c \sim 1.15$.

Phase-averaged vorticity fields at the top and bottom of the motion are shown in Figs 5–8. Figure 5a is for a Strouhal number of $Sr_c = 0.125$. This Strouhal number is associated with a significant increase in C_l when compared to the stationary value, but still relatively small when compared to higher Strouhal numbers. The flow field exhibits an oscillating shear layer of negative vorticity emanating from the leading-edge, and one of positive vorticity emanating from the trailing-edge. With the frequency increased to $Sr_c = 0.250$, the oscillating shear layer rolls up into multiple coherent vortices. The animations show these multiple vortices amalgamating so that at mid-way through the downstroke only two remain (not shown here). The passing of these two vortices over the trailing edge initiates the formation of two trailing edge vortices (TEVs) of opposite sign; the first of which is shown in Fig 5b at the bottom of the motion and the second is shown at the top of the motion.

With increasing Strouhal number the size and strength of the leading edge vortices (LEVs) and TEVs continue to increase as demonstrated for $Sr_c = 0.375$ and $Sr_c = 0.500$ by Fig 5c and d. This is reflected in the continued increase in C_l which levels out at $Sr_c = 0.500$ creating a local maximum. One possible explanation for this local maximum is the effect of the TEV. One would anticipate that during the upward motion of the airfoil a clockwise vortex would form below the trailing-edge, however Figure 5d demonstrates the opposite, a counterclockwise vortex above the trailing-edge. This discrepancy is due to the passing LEV initiating the TEV formation prematurely. Once formed the TEV is then reinforced during the downward motion by the lower surface shear layer, forming a strong vortex that exists for half the cycle. With the Strouhal number increased to $Sr_c = 0.625$ the LEV has not yet passed over the trailing-edge (see Fig. 6a), and the strong TEV has therefore not yet formed. It is therefore possible that the local maximum at $Sr_c = 0.500$ is a result of the TEV contributing less towards lift at higher Strouhal numbers, such as $Sr_c = 0.625$. The same peak at $Sr_c = 0.500$ is observed for other amplitudes and Reynolds numbers as demonstrated later in this paper. This phenomenon of an optimal vortex convection time scale has previously been described experimentally for an unsteady freestream by Gursul & Ho[22] and computationally for a plunging NACA 0012 by Andro & Jacquin[23]. An alternative explanation for the local maximum is presented in section B.

The continued rise in C_l beyond $Sr_c = 0.625$ is associated with the increasing strength of the LEV as demonstrated in Fig. 6, and quantified through the circulation calculations shown in Fig. 9a. Figure 9a and 9b show the circulation of the upper surface LEV from its inception at the leading-edge until it reaches the trailing-edge. For the lower Strouhal numbers shown in Figure 9a, the growth of the LEV is apparent in the range $t/T = 0.125$ to 0.375. One contributory factor to the increasing lift across this Strouhal number range is the increasing strength of the LEV. This is apparent through the increasing peak circulation at $t/T = 0.375$ with increasing Strouhal number. A second contributory factor is the increasing 'lifespan' of the vortex (the time taken for the vortex to pass beyond the trailing-edge or to be dissipated), which varies from a minimum of $\Delta t/T = 0.750$ at $Sr_c = 0.500$ to a maximum of $\Delta t/T = 1.500$ at $Sr_c = 1.125$. The maximum of $\Delta t/T = 1.500$ means that for half of every cycle, two vortices exist over the upper surface; one forming at the leading-edge, and a second nearing the trailing-edge from the previous cycle. Figure 6 demonstrates the same effect through the position of the LEV over the upper surface, i.e., in Fig. 6a (left) the LEV is approximately at 1c, Fig. 6b it is at ~ 0.8c, Fig. 6c it is at ~0.6c, and Fig 6d it is at ~0.5c. The position of the LEV therefore implies a nearly constant vortex convection time scale. This is substantiated through detailed vortex tracking calculations (not shown here). As a result of the increased lifespan, the LEV would contribute towards lift for a greater proportion of the cycle.

This trend of increasing LEV circulation and further upstream LEV position with increasing Strouhal number continues until $Sr_c = 1.250$ where there is a marked change, see Fig. 7b. The LEV now remains over the upstream portion of the airfoil for the entire cycle. Consequently it is destroyed through impingement with the upward moving airfoil in the same manner as described by Cleaver et al.[6] and Visbal[7] producing what was termed a mode-2 flow field , i.e., one with no convected LEV. Figure 9b demonstrates this effect through the rapid decrease in circulation to near-zero values at time $t/T = 0.875$ for $Sr_c \leq 1.750$. Furthermore with increasing Strouhal number the onset of the vortex dissipation becomes earlier in the cycle so that for $Sr_c > 1.750$ the near-zero circulation values commence at $t/T = 0.750$.

At the trailing-edge there is also a marked change in the flow structure, see Fig. 8. With increasing Strouhal number the TEVs remain closer to the trailing-edge. Consequently their proximity satisfies the vortex-dipole formation criteria described by Godoy-Diana et al.[18]. The two vortices therefore form a dipole pair which convects away from the airfoil at an angle to the horizontal, thereby forming a deflected wake[18, 19, 24, 25]; this can be seen in the left column of Figure 8 and the animations for $Sr_c \geq 1.250$ (not shown here). Due to the direction of the deflected wake, it draws fluid from the lower surface of the airfoil thereby accelerating the fluid over the lower surface and aiding in the formation of a lower surface LEV. As demonstrated in Fig. 10 and Fig. 11 the strength of this lower surface LEV grows substantially with increasing Strouhal number. Figure 10 shows that the lower surface LEV

begins to form at the bottom of the motion, t/T = 0.500, growing in strength during the upward motion before reaching a maximum at t/T = 0.875, and then being dissipated in a similar manner to the upper surface LEV through impingement with the airfoil. The peak circulation shown in Figure 11 demonstrates the strength of the lower surface LEV increases significantly with Strouhal number so that the rate of increase exceeds that of the upper surface LEV. In addition, the lifespan of the upper surface LEV is decreasing within this range. Consequently when the effects of increasing lower surface LEV circulation and the dissipation of the upper surface LEV are combined the result is a pronounced and sudden fall in C_l. Indeed at $Sr_c = 1.75$ (shown in Fig. 8) the strength of the lower surface LEV has grown to such an extent that it negates the time-averaged lift enhancement entirely, returning the lift coefficient to a value approximate to the stationary one.

The mode-2 flow field does however have a beneficial effect on the drag / thrust characteristics as shown in Fig. 4. Until $Sr_c \sim 1$, any change in drag coefficient is relatively small, but for $Sr_c > 1$ the coefficient of drag decreases substantially, turning negative at $Sr_c \sim 1.2$, and then becoming thrust producing. $Sr_c \sim 1.2$ coincides with the beginning of the mode-2 wake.

B. Effect of Amplitude

Figure 12 shows the lift coefficient for four further amplitudes in addition to the original amplitude of a/c = 0.15. For $Sr_c < 1$ all amplitudes demonstrate qualitatively similar behavior to that previously discussed, i.e., steady rise with a local peak at $Sr_c \sim 0.5$ followed by a continued rise. In addition Figs 12a, b and c show further local lift peaks at $Sr_c \sim 1.2$ and 2.1. Previously the peak at $Sr_c \sim 0.5$ was attributed to the vortex convection time, however an alternative explanation is that all three peaks are related to wake instabilities in a similar manner to unsteady blowing/suction. These peaks could therefore correlate with the natural shedding frequency[26-28]. To quantify the most unstable frequency, hot-film measurements were taken across an array of eighteen points 1c to 3c downstream of the trailing edge for the stationary airfoil. A typical example is shown in Fig. 13a. The Strouhal number of natural vortex shedding in terms of Sr_d ($fc\sin\alpha/U_\infty$) was measured to be 0.215, which agrees well with the established[27-34] value of $Sr_d \sim 0.2$. In terms of Strouhal number based on chord, $Sr_d = 0.215$ equates to $Sr_c = 0.83$. Therefore, the peak at $Sr_c \sim 0.5$ could be the subharmonic of the natural shedding frequency, as it is established that resonance with the harmonics and subharmonic of the fundamental wake frequency is possible[27, 28]. However, the degree to which the most unstable frequency for a static wing correlates with that for an oscillating wing is open to debate. Since as demonstrated in Fig. 13b through oscillation the wake changes significantly, and therefore presumably changes the natural frequency also. Further measurements and analysis are required to validate this hypothesis.

Quantitatively the effect of amplitude on lift coefficient is significant, with greater lift enhancement for larger amplitudes. This is emphasized in Fig. 14 where instead of Strouhal number based on chord, Strouhal number based on amplitude (effectively plunge velocity) is considered. Figure 14 demonstrates that for low Sr_c, all the amplitudes converge onto the same approximate linear trend. At higher Strouhal numbers a fall in lift is observed which is typical of a developing mode-2 flow field. The point at which this fall occurs is also strongly amplitude dependent: $Sr_c \sim 1.10$ for a/c = 0.200, $Sr_c \sim 1.35$ for a/c = 0.150, $Sr_c \sim 1.90$ for a/c = 0.100, a weak fall at $Sr_c \sim 2.30$ for a/c = 0.050, and no clear fall in C_l for a/c = 0.025.

C. Effect of Reynolds Number

To confirm that the initial peak was dependent on Sr_c and not frequency, force measurements were repeated for a/c = 0.200 at Re = 20,000. Figure 15 demonstrates that to within the bounds of experimental uncertainty Reynolds number has a negligible effect, and that the initial peak is a valid aerodynamic phenomenon. The cause of the peaks however, whether by wake instabilities of vortex convection time scale, remains unclear.

IV. Conclusions

It has been shown that small-amplitude plunging motion can produce significant lift enhancement. The largest recorded improvement was a 300% increase compared to the value for a stationary airfoil, coinciding with a thrust coefficient of 0.75. This lift enhancement was primarily due to a leading edge vortex/vortices, and was Reynolds number independent in the range 10,000 to 20,000. The degree of lift enhancement was shown to have an approximately linear proportionality with plunge velocity, until the onset of the mode-2 flow field. For a mode-2 flow field the combined action of upper surface LEV dissipation, and increasing lower surface LEV strength causes a significant decrease in lift. The onset was found to be strongly amplitude dependent and nonexistent for very small amplitudes.

Multiple local peaks were observed in the lift data, independent of amplitude, at Sr_c = 0.5, 1.2 and 2.1. Two potential explanations were suggested. The initial peak at Sr_c = 0.5 could be attributed to the LEV vortex convection time scale, however this would not explain the latter peaks. The second explanation is that the local peaks are due to resonance with the harmonic and subharmonics of the most wake unstable frequency. This hypothesis is difficult to substantiate as the wake is substantially modified through oscillation therefore causing substantial changes in the theoretical unstable wake frequencies.

Acknowledgments

The authors would like to acknowledge the support from an EPSRC studentship, and the RCUK Academic Fellowship in Unmanned Air Vehicles.

V. References

[1]Pines, D.J. and Bohorquez, F. "Challenges facing future micro-air-vehicle development," *Journal of Aircraft*, Vol. 43, No. 2, 2006, pp. 290-305.

[2]Mueller, T.J. and DeLaurier, J.D. "Aerodynamics of small vehicles," *Annual Review of Fluid Mechanics*, Vol. 35, 2003, pp. 89-111.

[3]Ho, S., Nassef, H., Pornsinsirirak, N., Tai, Y.C. and Ho, C.M. "Unsteady aerodynamics and flow control for flapping wing flyers," *Progress in Aerospace Sciences*, Vol. 39, No. 8, 2003, pp. 635-681.

[4]Shyy, W., Berg, M. and Ljungqvist, D. "Flapping and flexible wings for biological and micro air vehicles," *Progress in Aerospace Sciences*, Vol. 35, No. 5, 1999, pp. 455-505.

[5]Taylor, G., Wang, Z., Vardaki, E. and Gursul, I. "Lift enhancement over flexible nonslender delta wings," *AIAA Journal*, Vol. 45, No. 12, 2007, pp. 2979-2993.

[6]Cleaver, D.J., Wang, Z.J. and Gursul, I. "Delay of Stall by Small Amplitude Airfoil Oscillation at Low Reynolds Numbers," 47th AIAA Aerospace Sciences Meeting, AIAA 2009-392, AIAA, 2009.

[7]Visbal, M.R. "High-Fidelity Simulation of Transitional Flows Past a Plunging Airfoil," 47th AIAA Aerospace Sciences Meeting, AIAA 2009-391, AIAA, 2009.

[8]Moffat, R.J. "Contributions to the Theory of Single-Sample Uncertainty Analysis," *Journal of Fluids Engineering-Transactions of the ASME*, Vol. 104, No. 2, 1982, pp. 250-260.

[9]Heathcote, S. "Flexible Flapping Airfoil Propulsion at Low Reynolds Numbers," Ph.D. Dissertation, Dept of Mechanical Engineering, University of Bath, Bath, 2006.

[10]Sunada, S., Yasuda, T., Yasuda, K. and Kawachi, K. "Comparison of wing characteristics at an ultralow Reynolds number," *Journal of Aircraft*, Vol. 39, No. 2, 2002, pp. 331-338.

[11]Sunada, S., Sakaguchi, A. and Kawachi, K. "Airfoil section characteristics at a low Reynolds number," *Journal of Fluids Engineering-Transactions of the Asme*, Vol. 119, No. 1, 1997, pp. 129-135.

[12]Tsang, K.K.Y., So, R.M.C., Leung, R.C.K. and Wang, X.Q. "Dynamic stall behavior from unsteady force measurements," *Journal of Fluids and Structures*, Vol. 24, No. 1, 2008, pp. 129-150.

[13]Chen, J.M. and Choa, C.C. "Freestream disturbance effects on an airfoil pitching at constant rate," *Journal of Aircraft*, Vol. 36, No. 3, 1999, pp. 507-514.

[14]McKinney, W.D., J.;. "The Wingmill: An Oscillating-Wing Windmill," *Journal of Energy*, Vol. 5, No. 2, 1981, pp. 109-115.

[15]Frampton, K.D., Goldfarb, M., Monopoli, D. and Cveticanin, D. "Passive aeroelastic tailoring for optimal flapping wings," Proceedings of Conference on Fixed, Flapping and Rotary Wing Vehicles at Very Low Reynolds Numbers, 2000, pp. 473-482.

[16]Graftieaux, L., Michard, M. and Grosjean, N. "Combining PIV, POD and vortex identification algorithms for the study of unsteady turbulent swirling flows," *Measurement Science & Technology*, Vol. 12, No. 9, 2001, pp. 1422-1429.

[17]Morgan, C.E., Babinsky, H. and Harvey, J.K. "Vortex Detection Methods for use with PIV and CFD data," 47th AIAA Aerospace Sciences Meeting, AIAA 2009-74, AIAA, 2009.

[18]Godoy-Diana, R., Marais, C., Aider, J.L. and Wesfreid, J.E. "A model for the symmetry breaking of the reverse Benard-von Karman vortex street produced by a flapping foil," *Journal of Fluid Mechanics*, Vol. 622, 2009, pp. 23-32.

[19]Jones, K.D., Dohring, C.M. and Platzer, M.F. "Experimental and computational investigation of the Knoller-Betz effect," *AIAA Journal*, Vol. 36, No. 7, 1998, pp. 1240-1246.

[20]Young, J. and Lai, J.C.S. "Oscillation frequency and amplitude effects on the wake of a plunging airfoil," *AIAA Journal*, Vol. 42, No. 10, 2004, pp. 2042-2052.

[21]Triantafyllou, M.S., Triantafyllou, G.S. and Gopalkrishnan, R. "Wake Mechanics for Thrust Generation in Oscillating Foils," *Physics of Fluids a-Fluid Dynamics*, Vol. 3, No. 12, 1991, pp. 2835-2837.

[22]Gursul, I., Lin, H. and Ho, C.M. "Effects of Time Scales on Lift of Airfoils in an Unsteady Stream," *AIAA Journal*, Vol. 32, No. 4, 1994, pp. 797-801.

[23]Andro, J.Y. and Jacquin, L. "Frequency effects on the aerodynamic mechanisms of a heaving airfoil in a forward flight configuration," *Aerospace Science and Technology*, Vol. 13, No. 1, 2009, pp. 71-80.

[24]Heathcote, S. and Gursul, I. "Jet switching phenomenon for a periodically plunging airfoil," *Physics of Fluids*, Vol. 19, No. 2, 2007.

[25]von Ellenrieder, K.D. and Pothos, S. "PIV measurements of the asymmetric wake of a two dimensional heaving hydrofoil," *Experiments in Fluids*, Vol. 44, No. 5, 2008, pp. 733-745.
[26]Seifert, A. and Pack, L.G. "Oscillatory control of separation at high Reynolds numbers," *AIAA Journal*, Vol. 37, No. 9, 1999, pp. 1062-1071.
[27]Wu, J.Z., Lu, X.Y., Denny, A.G., Fan, M. and Wu, J.M. "Post-stall flow control on an airfoil by local unsteady forcing," *Journal of Fluid Mechanics*, Vol. 371, 1998, pp. 21-58.
[28]Miranda, S., Vlachos, P.P., Telionis, D.P. and Zeiger, M.D. "Flow control of a sharp-edged airfoil," *AIAA Journal*, Vol. 43, No. 4, 2005, pp. 716-726.
[29]Huang, R.F. and Lin, C.L. "Vortex Shedding and Shear-Layer Instability of Wing at Low-Reynolds Numbers," *AIAA Journal*, Vol. 33, No. 8, 1995, pp. 1398-1403.
[30]Abernathy, F.H. "Flow Over an Inclined Plate," *Transactions of the ASME, Journal of Basic Engineering*, Vol. 84, 1962, pp. 380 - 388.
[31]Fage, A. and Johansen, F.C. "On the Flow of Air Behind an Inclined Flat Plate of Infinite Span," *Proceedings of the Royal Society of London Series A*, Vol. 116, 1927, pp. 170-197.
[32]Hoarau, Y., Braza, M., Ventikos, Y., Faghani, D. and Tzabiras, G. "Organized modes and the three-dimensional transition to turbulence in the incompressible flow around a NACA0012 wing," *Journal of Fluid Mechanics*, Vol. 496, 2003, pp. 63-72.
[33]Huang, R.F. and Lee, H.W. "Turbulence effect on frequency characteristics of unsteady motions in wake of wing," *AIAA Journal*, Vol. 38, No. 1, 2000, pp. 87-94.
[34]Yeung, W.W.H. "Self-similarity of confined flow past a bluff body," *Journal of Wind Engineering and Industrial Aerodynamics*, Vol. 96, No. 4, 2008, pp. 369-388.

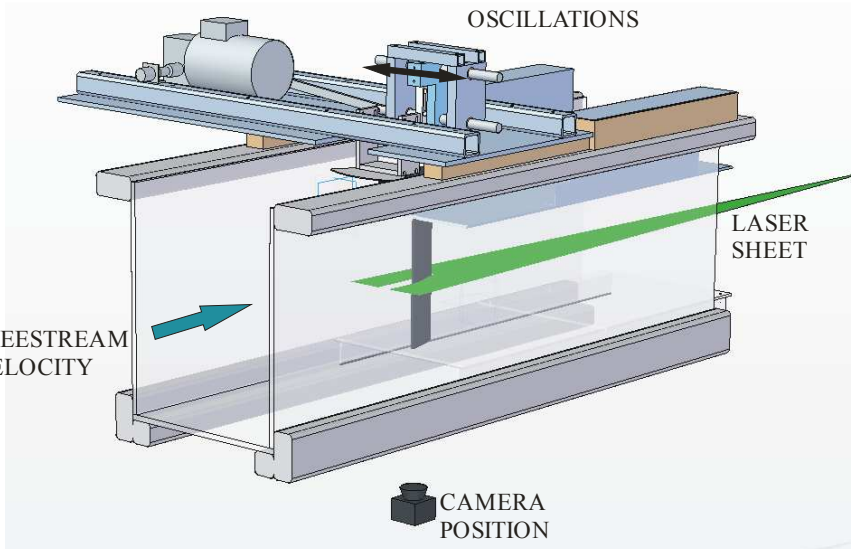

Figure 1. Experimental setup

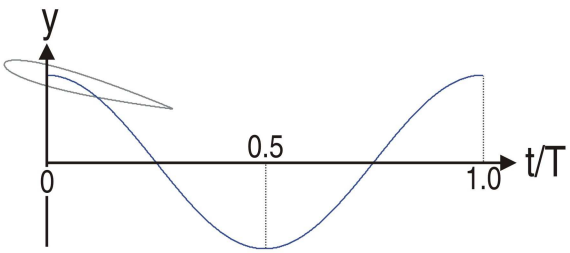

Figure 2. Schematic of the plunging motion

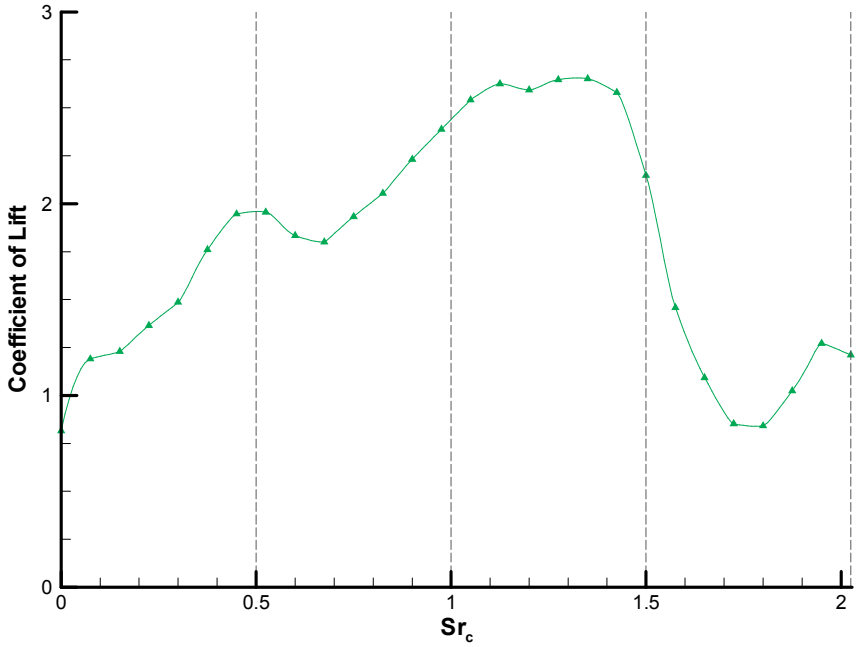

Figure 3. Lift coefficient vs. Sr_c for a/c=0.15, α=15°, Re=10,000. Dashed lines denote regions for PIV data shown in Fig.s 5 to 8.

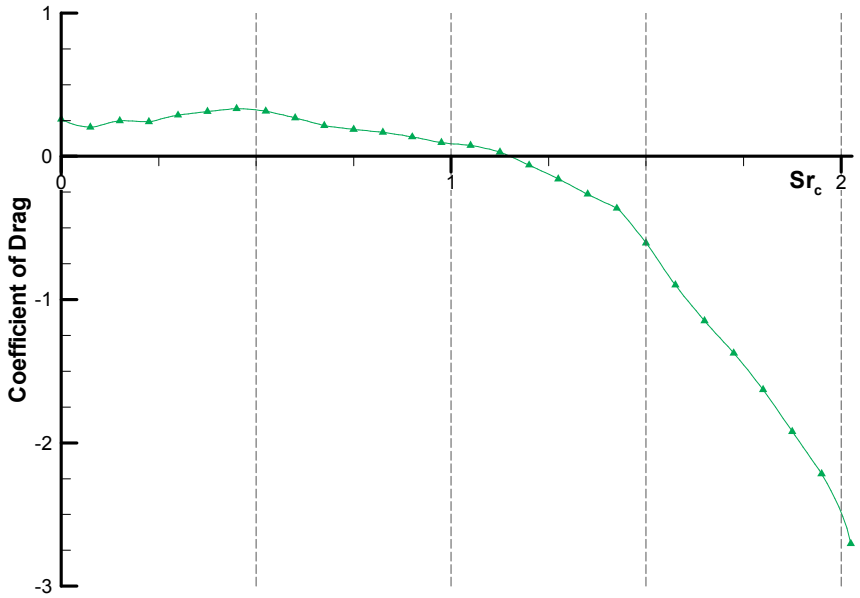

Figure 4. Drag coefficient vs. Sr_c for a/c=0.15, α=15°, Re=10,000. Dashed lines denote regions for PIV data shown in Fig.s 5 to 8.

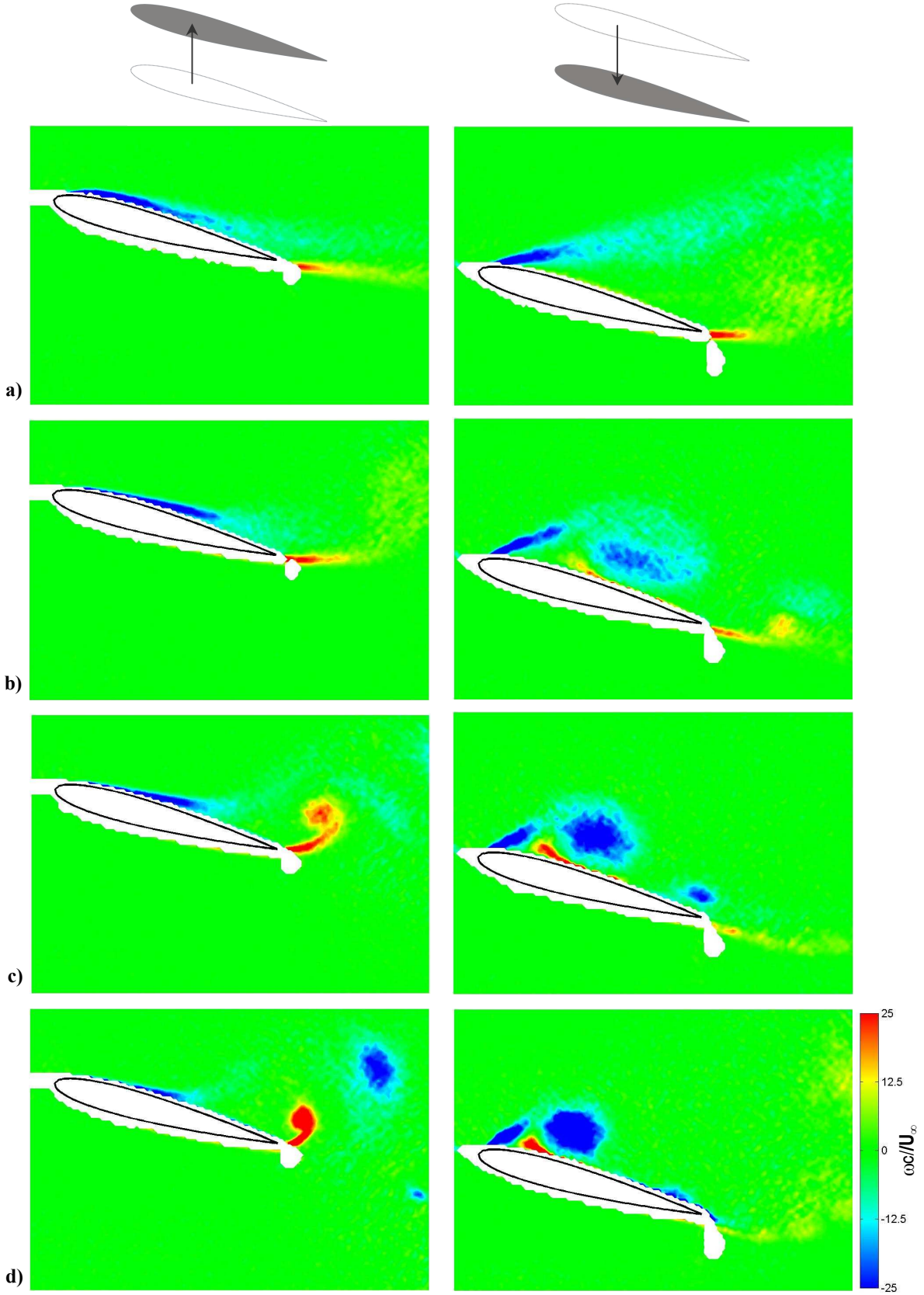

Figure 5. Normalized vorticity at maximum (left) and minimum (right) of motion with a/c = 0.15, α = 15°, Re = 10,000, for: a) $Sr_c = 0.125$, b) $Sr_c = 0.250$, c) $Sr_c = 0.375$, d) $Sr_c = 0.500$.

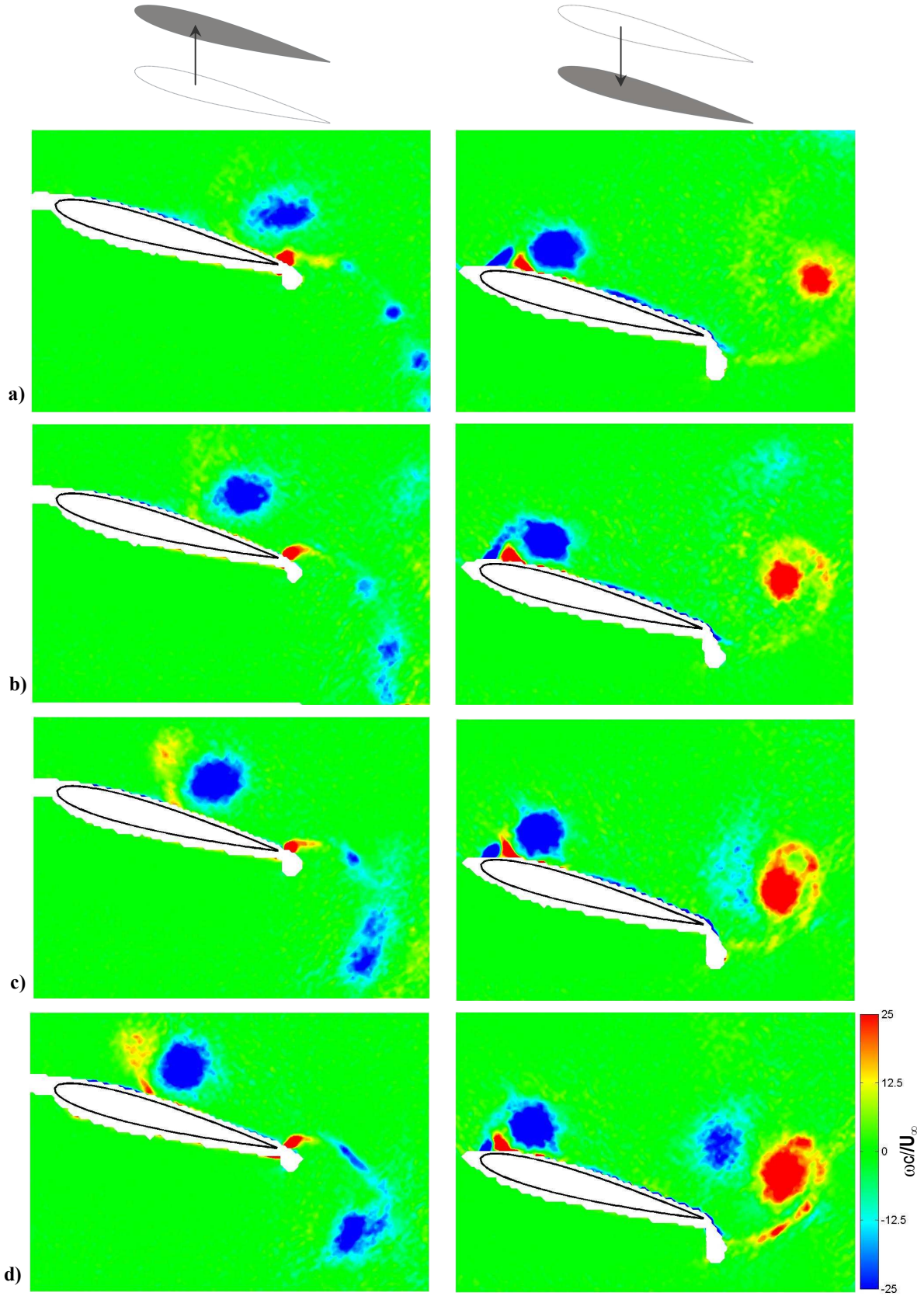

Figure 6. Normalized vorticity at maximum (left) and minimum (right) of motion with a/c = 0.15, α = 15°, Re = 10,000, for: a) $Sr_c = 0.625$, b) $Sr_c = 0.750$, c) $Sr_c = 0.875$, d) $Sr_c = 1.000$.

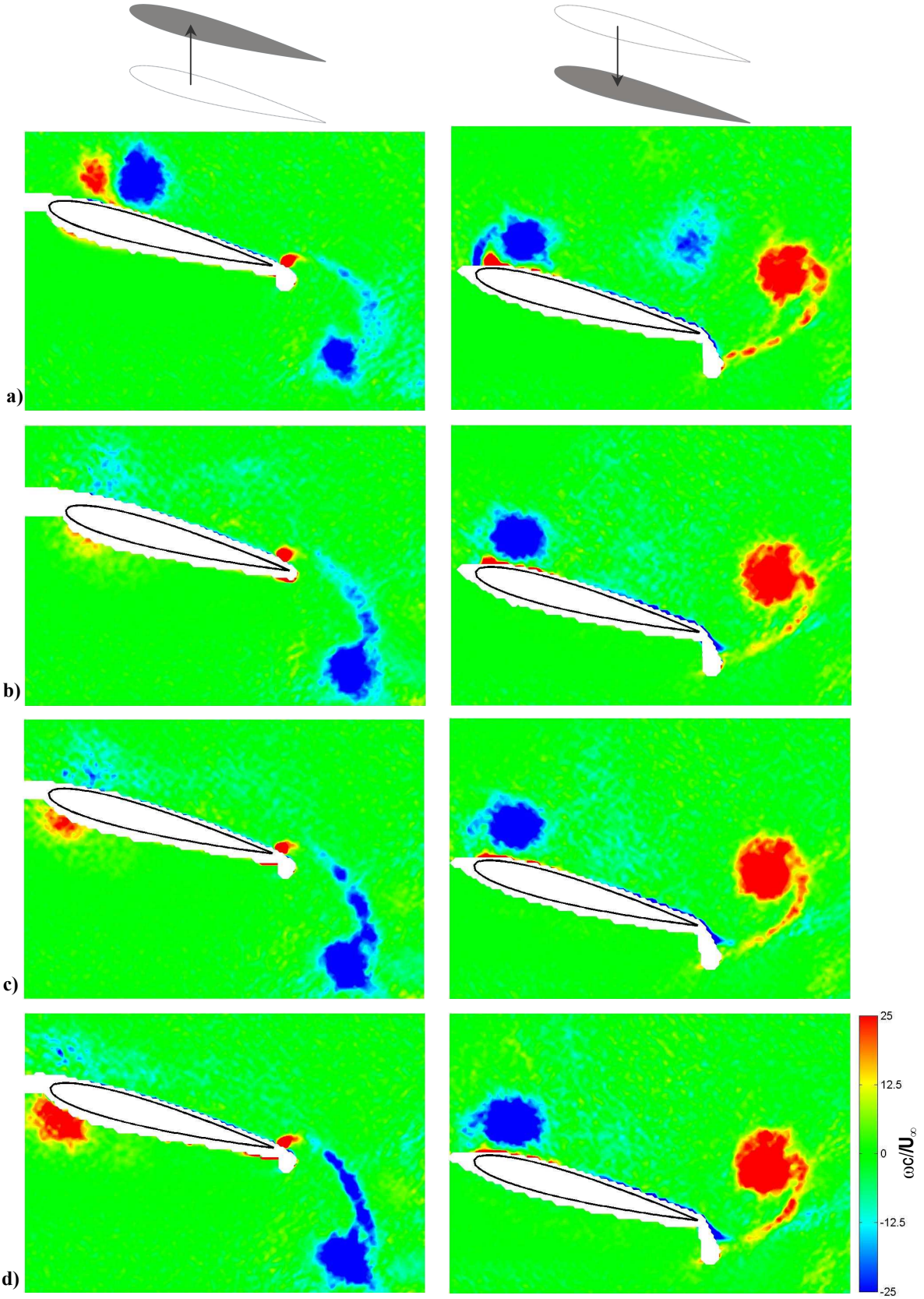

Figure 7. Normalized vorticity at maximum (left) and minimum (right) of motion with a/c = 0.15, α = 15°, Re = 10,000, for: a) $Sr_c = 1.125$, b) $Sr_c = 1.250$, c) $Sr_c = 1.375$, d) $Sr_c = 1.500$.

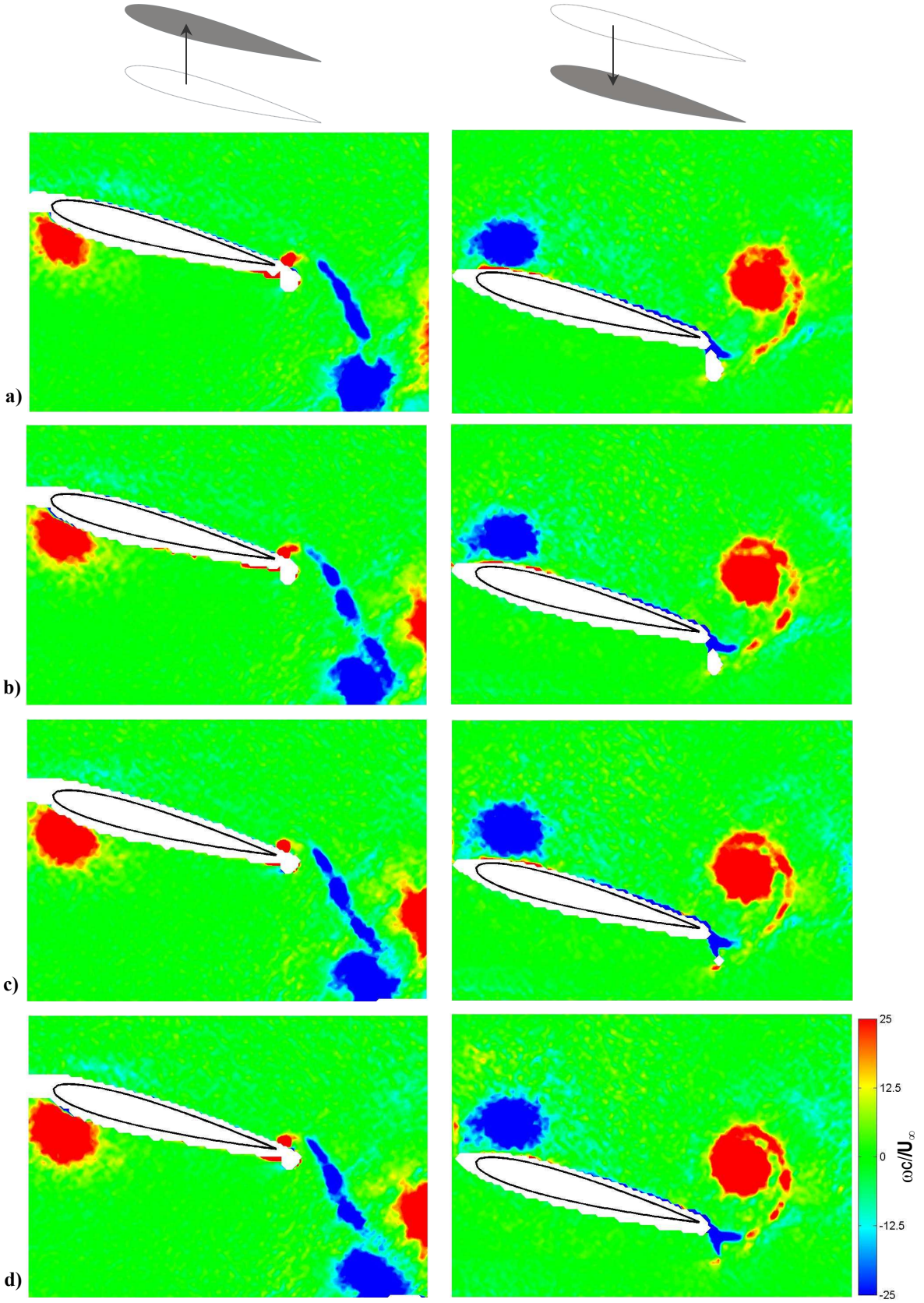

Figure 8. Normalized vorticity at maximum (left) and minimum (right) of motion with a/c = 0.15, α = 15°, Re = 10,000, for: a) Sr_c = 1.625, b) Sr_c = 1.750, c) Sr_c = 1.875, d) Sr_c = 2.000.

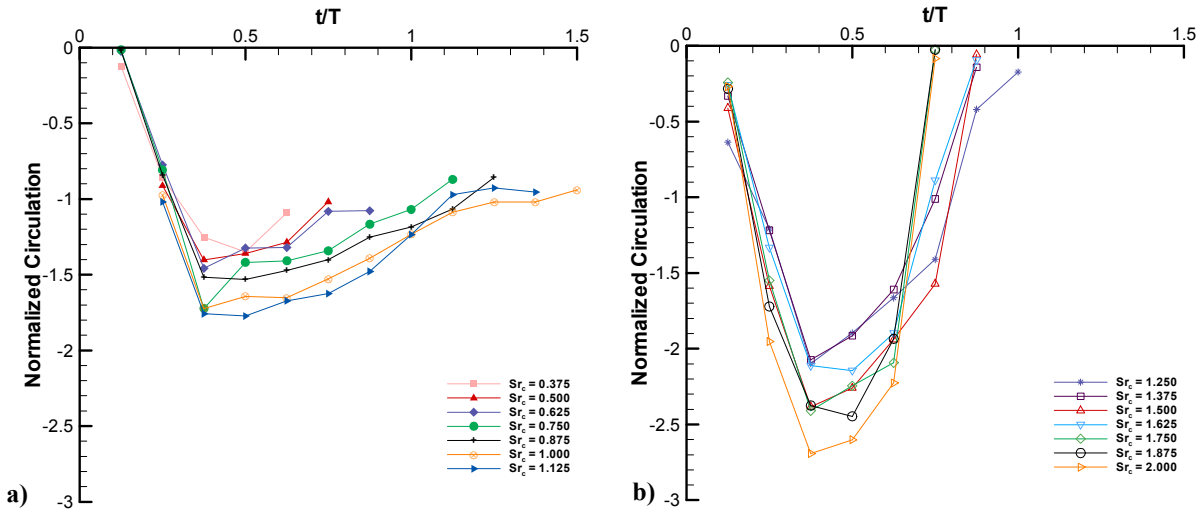

Figure 9. LEV circulation for upper surface for: a) $Sr_c \leq 1.125$, b) $Sr_c \geq 1.250$

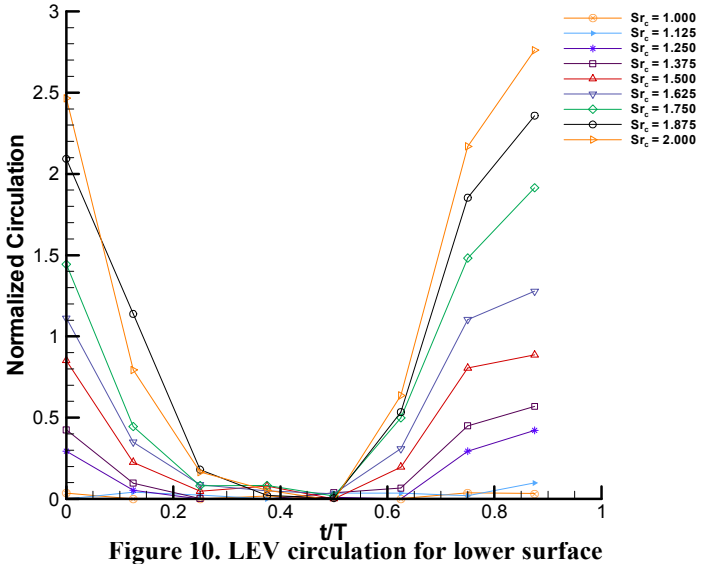

Figure 10. LEV circulation for lower surface

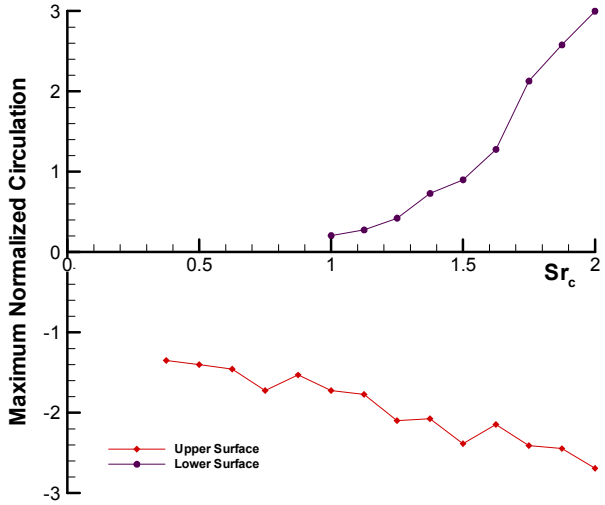

Figure 11. Peak circulation for upper and lower surface

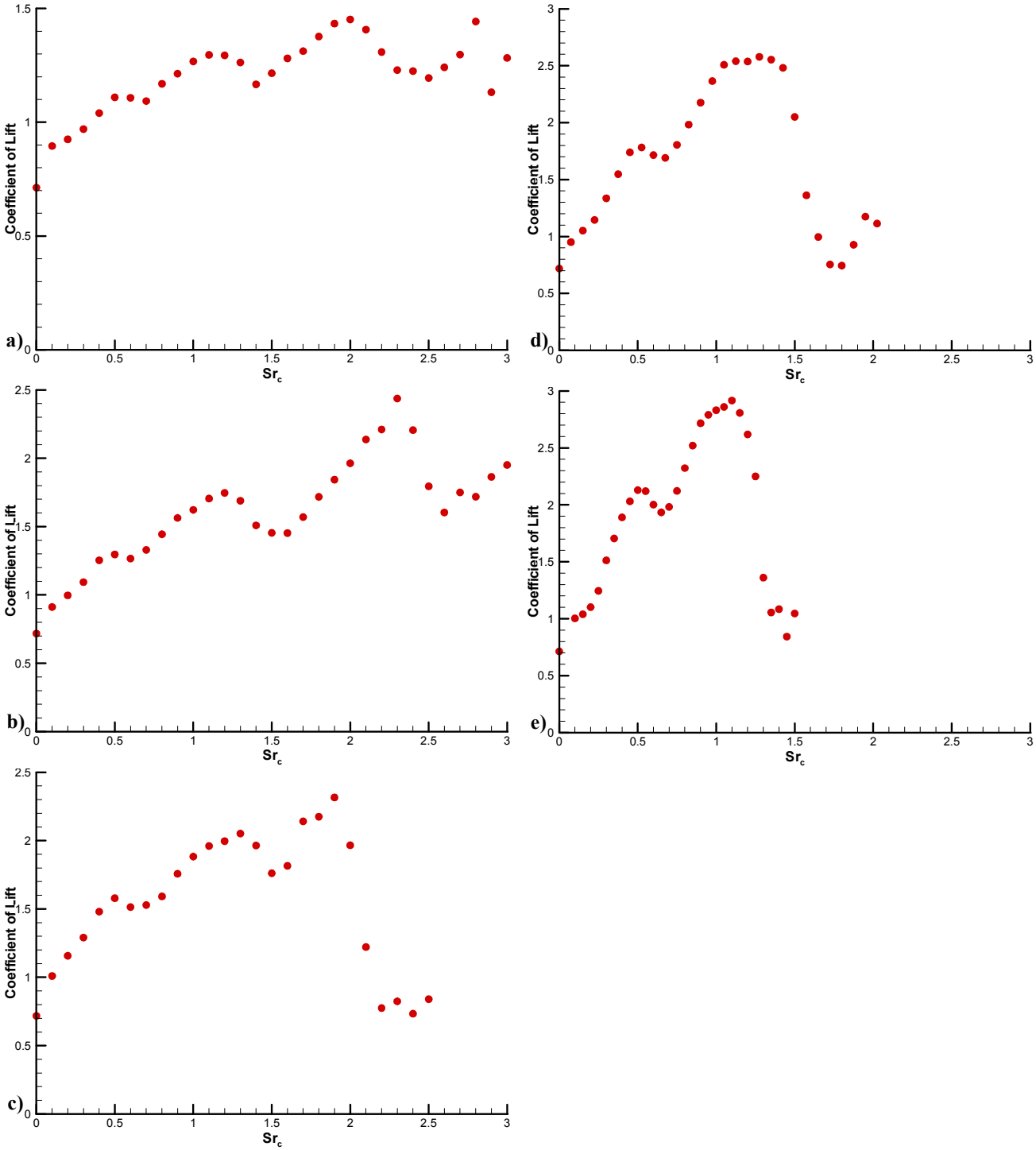

Figure 12. Effect of amplitude on lift coefficient. α = 15°, Re = 10,000, for: a) a/c = 0.025, b) a/c = 0.050, c) a/c = 0.100, d) a/c = 0.150, e) a/c = 0.200.

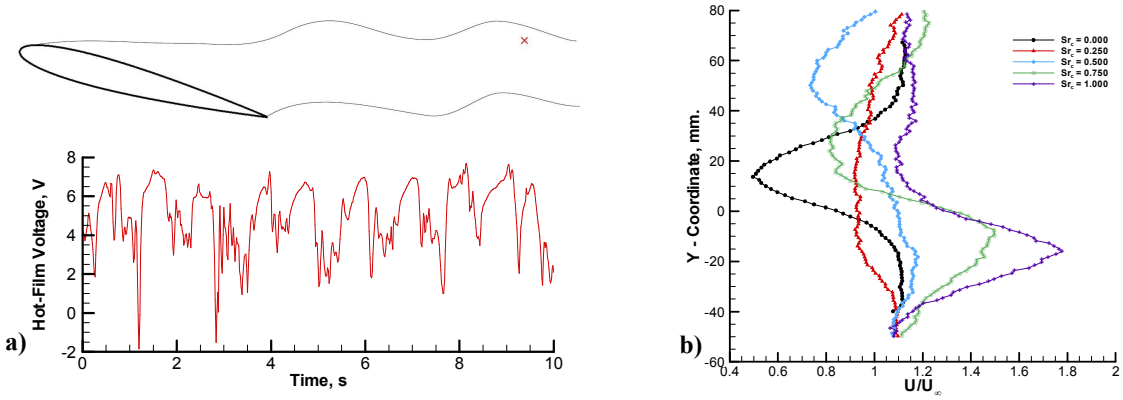

Figure 13. a) Hot-film signal in the wake of the stationary airfoil; cross denotes the location of measurement, b) time-averaged streamwise velocity measured through PIV 0.75c downstream of the trailing edge, Y-coordinate is relative to the trailing edge.

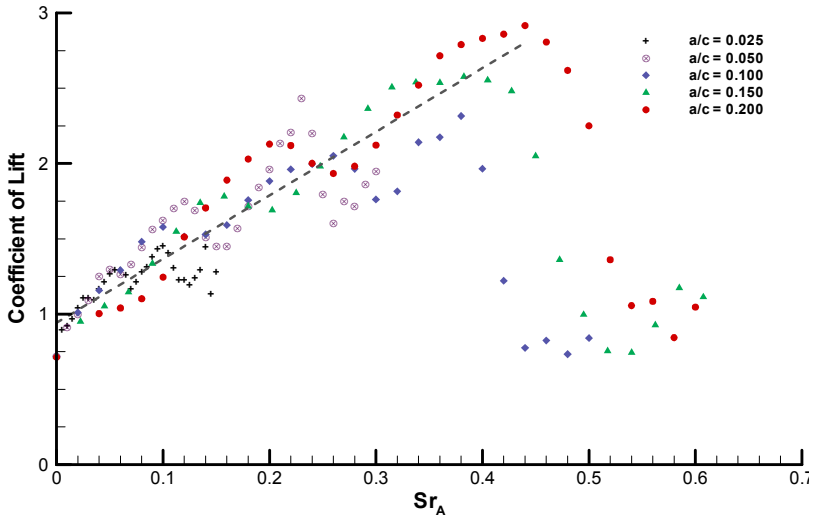

Figure 14. Lift coefficient vs. Strouhal number based on amplitude. Dashed line denotes line of best fit.

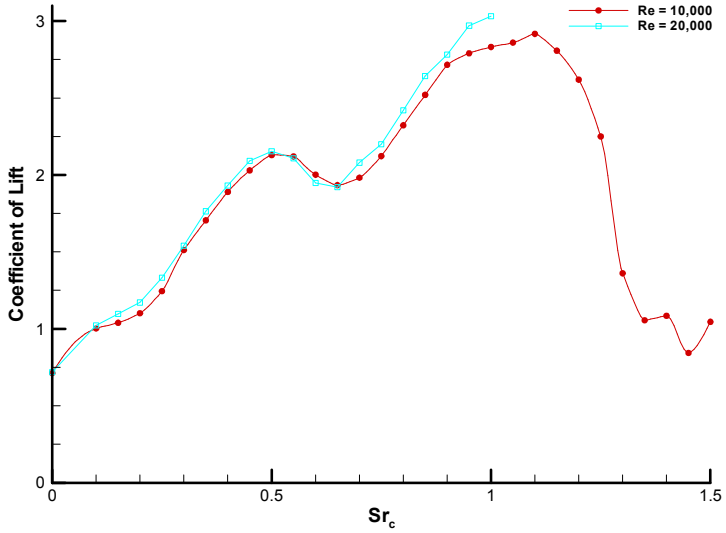

Figure 15. Effect of Reynolds number, for a/c = 0.200 at Re = 10,000 and 20,000.